7404 *Macromolecules* **2009**, *42*, 7404–7412
DOI: 10.1021/ma901137g

Macromolecules
ARTICLE

Local Water Dynamics in Coacervated Polyelectrolytes Monitored through Dynamic Nuclear Polarization-Enhanced ^{1}H NMR

Ravinath Kausik,[†,‡] Aasheesh Srivastava,[†,‡,§] Peter A. Korevaar,[†,‡,⊥] Galen Stucky,[†,‡] J. Herbert Waite,[†,‡,§] and Songi Han*[,†,‡]

[†]*Department of Chemistry and Biochemistry, University of California, Santa Barbara, California 93106,* [‡]*Materials Research Laboratory, University of California, Santa Barbara, California 93106, and* [§]*Molecular Cellular and Developmental Biology, University of California, Santa Barbara, California 93106.* [⊥] *Present address: Institute for Complex Molecular Systems, Eindhoven University of Technology, PO Box 513, 5600 MB, The Netherlands.*

Received May 26, 2009; Revised Manuscript Received August 13, 2009

ABSTRACT: We present the first study of quantifying the diffusion coefficient of interfacial water on polyelectrolyte surfaces of systems fully dispersed in bulk water under ambient conditions. Such measurements were made possible through the implementation of a recently introduced dynamic nuclear polarization (DNP) technique to selectively amplify the nuclear magnetic resonance (NMR) signal of hydration water that is interacting with specifically located spin-labels on polyelectrolyte surfaces. The merit of this novel capability is demonstrated in this report through the measurement of solvent microvisosity on the surface of two types of oppositely charged polyelectrolytes: when freely dissolved versus when complexed to form a liquid−liquid colloidal phase called complex coacervates. These complex coacervates were formed through electrostatic complexation between the imidazole-based cationic homopolymer poly(*N*-vinylimidazole) (PVIm) and anionic polypeptide polyaspartate (PAsp) in the pH range of 4.5−6.0, under which conditions the coacervate droplets are highly fluidic yet densely packed with polyelectrolytes. We also investigated the rotational diffusion coefficients of the spin-labels covalently bound to the polyelectrolyte chains for both PVIm and PAsp, showing a 5-fold change in the rotational correlation time as well as anisotropy parameter upon coacervation, which represents a surprisingly small decrease given the high polymer concentration inside the dense microdroplets. For both DNP and ESR experiments, the polymers were covalently tagged with stable nitroxide radical spin-labels (∼1 wt %) to probe the local solvent and polymer segment dynamics. We found that the surface water diffusion coefficients near uncomplexed PVIm and PAsp at pH 8 differ and are around $D \sim 1.3 \times 10^{-9}$ m^2/s. In contrast, inside the complex coacervate phase, the water diffusion coefficient in the immediate vicinity of either polyelectrolyte was $D \sim 0.25 \times 10^{-9}$ m^2/s, which is about an order of magnitude smaller than the bulk water self-diffusion coefficient and yet orders of magnitude greater than that of associated, bound, hydration water. This observation suggests the existence of measurable water inside complex coacervates with relatively high diffusion and exchange dynamics, implying that water moves in nanometer-scale pore spaces as opposed to being structurally bound or even absent. We infer from our observation that the PVIm and PAsp chains are undergoing roughly pairwise association, so that largely charge-neutralized species compose the concentrated, yet fluidic, and partially hydrated coacervate cores.

1. Introduction

Complex coacervation is a liquid−liquid phase separation of oppositely charged polyelectrolytes, i.e., polycations and polyanions.[1,2] These polyelectrolyte complexes segregate into coacervate droplets that further coalesce to form a separate dense bulk phase with significantly higher polymer concentration and viscosity compared to the original polyelectrolyte solutions. The process was first seen by Tiebackx[3] and later termed complex coacervation by Bungenberg de Jong and Kruyt[4] after a systematic investigation of the system of gum arabic and gelatin.

The applications of complex coacervation have impacted various fields. Oparin suggested complex coacervation to be the mechanism behind the separation of a fluid phase distinct from the "primordial soup" in his famous theory of the *origin of life* on earth.[5] From a practical point of view complex coacervation has found uses in processed food,[6] biomaterials,[7] cosmetics, and also in carbon-less paper.[8] Additional applications of complex coacervation include those in pharmaceutical and food industries where they are used as microencapsulates for insoluble materials like drugs and flavors,[9−13] thus making them promising candidates for various applications dealing with targeted drug delivery and controlled permeability. It has recently been reported that complex coacervation plays a key role in the coating, building, and the adhesive functions of marine organisms.[14,15] What makes this phenomenon intriguing and unique for a wide range of problems are the peculiar dynamic properties of these dense polymer droplets. Yet, there are only a few systematic studies on the physical characterization of complex coacervates, fewer on the rotational diffusion coefficients of polyelectrolytes, and none on the quantitative determination of the presence and dynamics of solvent water within complex coacervates. The relevance of the various dynamic parameters, the challenges of analyzing dynamic properties of complex coacervates, and our unique magnetic resonance approach to measure microviscosities will be discussed in the following sections. The main questions that we seek to answer in this study are (1) what is the solvent microviscosity, (2) what is the change in polyelectrolyte mobility

*Corresponding author. E-mail: songi@chem.ucsb.edu.

 Published on Web 08/31/2009

upon coacervation, and finally (3) what can we learn regarding the molecular organization or structure of the polyelectrolytes from the dynamic properties of these systems?

The formation of the electrostatic complexes between two oppositely charged polymers can be fine-tuned through parameters that influence the strength of the interpolymer electrostatic interactions, such as pH, salt concentration, chain length, and ionic strength of the polyelectrolytes.[1,6] A thorough and systematic understanding of complex coacervation has been hindered by the complex and varied chemical compositions and structures of the macromolecules involved. Lack of chromophores in natural biopolymers, strong scattering by the coacervate phase, and the dynamic nature of the condensation of the polymers to varied sizes of liquid droplets further aggravate these difficulties. There have been reports in the literature on the attempts to study the coacervate chain dynamics by techniques including NMR, ESR, fluorescence, FRAP, and various scattering techniques,[16−18] which has led to the understanding of kinetics of polyelectrolyte complexation. There have also been attempts to introduce improved techniques like X-ray reflectivity, diffusion wave spectroscopy, and confocal scanning laser microscopy for investigating coacervation.[19,20] Nonetheless, the fundamental structure-dynamic properties of complex coacervates especially with regards to solvent dynamics within coacervates remain poorly quantified.

Coacervates have been found to be dense aggregates of the complexed polyelectrolytes. However, these aggregates can be uniform or nonuniform depending on the system under consideration. Some of the interesting reports on the existence of pores or heterogeneities in complex coacervates include the spongelike morphology observed in randomly branched gels of poly(glutamic acid)/dendrimer coacervates,[21] vacuoles of entrapped solvent in the coacervate systems of α-lactoglobulin (α-lg)/gum Arabic (GA),[8] and the spongelike vesicle structures in a purely synthetic system of zwitterionic gemini surfactants in water.[22,23] These recent studies provide insight that coacervates can be water-filled porous structures, but there is no quantitative study on the presence and dynamics of this water. An improved quantitative understanding of these properties, especially as a function of polyelectrolyte structure, is required. The understanding of the local solvent dynamics is important because it determines the effective response of complex coacervates to solvent-mediated stimuli, such as pH or salt, and therefore influences how well they serve as cell mimetic or tissue culture media. The main challenges in understanding the dynamics of the solvent molecules close to the polyelectrolyte surface lie in separately observing this locally interacting water from the bulk solvent molecules. While there have been some studies on boundary-layer water in other systems such as the surface of protein molecular assemblies (e.g., by IR and near-IR vibrational spectroscopy[24] and magnetic resonance methods[25−27]), there are no reports on the nature of the water locally interacting with the surface of the polyelectrolyte in the extended uncoacervated or the compact coacervated state, nor is there an evaluation of the diffusion constants of these local water molecules on the surface of any macromolecular system or complexes.

In this paper we present the development and application of a new experimental technique to access the water that is locally interacting with the polyelectrolyte surface and to quantify its local diffusion coefficients. Using a magnetic resonance principle termed dynamic nuclear polarization (DNP), we transfer magnetization from the free electrons of spin-labels which are covalently tethered to the polyelectrolytes to the ^{1}H nuclei of the solvent water. This process utilizes the ∼658-fold higher spin polarization of electron spins compared to ^{1}H nuclei. The dominant mechanism of this DNP transfer is the Overhauser effect, which produces amplification of the ^{1}H NMR signal of solvent water through the modulation of the dipolar interactions between the water protons and the free radical electrons of the spin-labels.[28] For our system of ^{1}H nuclei of water dynamically interacting with stable nitroxide species it has been shown that dipolar relaxation is dominated by translational motion of the interacting species.[29] Thus, the DNP-amplified ^{1}H NMR signal is predominantly sensitive to the translational fluid dynamics of water directly interacting with the spin-label. As 80% of the dipolar interactions between the ^{1}H water protons and free electrons of the spin-labels come from within 5 Å distance from the spin-label (due to dipolar interactions rapidly falling off with distance[30]), this effect measures the characteristics of truly local water interacting with the spin-label probe. We have demonstrated that this technique can be used to quantify the local water self-diffusion coefficients around biological systems,[31,32] which is possible because the water dynamics within 5−10 Å of the spin-label is not altered from the bulk water dynamics through the mere presence of spin-labels.[33] Here, the unique and most important feature of our approach is that the interfacial property of biomolecules in dilute solutions (a few hundred μM) and small quantities (3−4 μL) can be measured. Finally, because the DNP analysis of hydration water is performed through a site-specific spin-label, the very same spin probes can be employed for electron spin resonance (ESR) analysis of the rotational diffusion of the spin-label and the polyelectrolyte segment that it is attached to. Because the sensitivities of DNP and ESR analyses are comparable, both the microviscosity of the solvent and the coupled rotational diffusion of spin-labels and the polymer segments can be measured for the same sample in situ. We chose a system of two simple homopolyelectrolytes, polyvinylimidazole (PVIm) and polyaspartate (PAsp), functionalized with spin-labels at ∼1 wt % concentration. The DNP and ESR analyses of complex coacervates are carried out with either the PVIm or PAsp carrying spin-labels, so that the solvent and polymer dynamics can be observed from the perspective of both polycations and polyanions.

2. Experimental Methods

2.1. Polymer Synthesis and Functionalization. Postsynthetic modification of the imidazole groups in PVIm was undertaken to attach the ESR spin-label 2,2,6,6-tetramethylpiperidine-*N*-oxyl (TEMPO). The polymer in the present study was synthesized through simple free-radical polymerization as reported previously.[34] PVIm is a homopolymer model protein having a polycarbon backbone and multiple imidazole pendants. 4-(2-Iodoacetamido)-TEMPO was used for covalently attaching TEMPO groups to PVIm by the nucleophilic attack of imidazole on the electron-deficient iodoacetamido group, as described below. In a separate synthetic protocol to prepare the anionic polymer counterpart, the polysuccinimide precursor to polyaspartate was prepared by thermal polymerization of aspartic acid in the presence of orthophosphoric acid (synthesis details given below). The polysuccinimide precursor can undergo nucleophilic reaction with amines.[35] Thus, mild heating of polysuccinimide with 4-amino-TEMPO resulted in the attachment of TEMPO groups to the polysuccinimide through an amide linkage. The product was purified by a combination of precipitation and dialysis to remove any unreacted TEMPO precursor. The rest of the succinimide groups were opened using aqueous sodium hydroxide solution to obtain TEMPO-labeled polyaspartate. For preparing unlabeled polyaspartate, the polysuccinimide was directly subjected to base hydrolysis. The conversion of succinimide to carboxylates was evident from the free solubility of the product in water, in contrast to the precursor that was insoluble in water.

Preparation of TEMPO-Labeled PVIm. Following Scheme 1, PVIm (74 kDa) (218.3 mg, 2.3 mmol) was dissolved in 4 mL of

ethanol under magnetic stirring at room temperature. In a separate vial, 4-(2-iodoacetamido)-2,2,6,6-tetramethylpiperidine-*N*-oxide (TEMPO) (11.8 mg, 35 μmol) was dissolved in chloroform (0.5 mL) and added dropwise into the PVIm ethanolic solution. This mixture was stirred overnight and concentrated in vacuum, and the product was precipitated by addition of acetone (10 mL). The precipitate was dried under vacuum to obtain an off-white solid.

Preparation of TEMPO-Labeled PAsp. Sodium polyaspartate was synthesized according to an established procedure reported in the literature.[35] Briefly, a paste of aspartic acid (3 g) and orthophosphoric acid (3 mL) was heated at 180 °C at 100 mmHg vacuum for 3 h (Scheme 2). The resultant viscous liquid was poured into cold water to isolate the polysuccinimide intermediate as a white solid. After filtration and drying, 200 mg of this polysuccinimide was suspended in 3 mL of DMF. To the turbid mixture, 6 mg of 4-aminoTEMPO dissolved in 100 μL of DMF was added. This mixture was kept for heating at 50 °C for 36 h to obtain a clear pink solution. This solution was poured into 0.1 N HCl solution and centrifuged at 2000 rpm for 10 min to obtain a light yellow precipitate. The precipitate was further rinsed twice with water (5 mL) and dissolved in 0.1 M NaOH solution (2 mL). This basic solution of the polymer was dialyzed against water for 24 h using a cellulose acetate membrane with MWCO of 10 kDa. Lyophilization of the resulting pale brown solution resulted in the isolation of 128 mg of TEMPO-labeled polyaspartate (60 kDa) as a light brown solid.

Complex Coacervation of PVIm and PAsp. Complex coacervation was induced by mixing the aqueous solutions of PVIm and PAsp (50 mM final concentration) at pH 9 and then reducing pH of the resulting solution by addition of 2% HCl. An immediate increase in turbidity of the sample was observed uniformly throughout the sample as the pH was decreased to 6.5 (Figure 1). The turbidity indicates the onset of the formation of complex coacervates. The solution remains turbid until about a pH of 4.5 and then starts getting clear again when the pH drops below 4.5. The presence of microscopic complex coacervate aggregates was confirmed by differential interference contrast optical microscopy (Figure 2).

Scheme 1. Preparation of TEMPO-Labeled PVIm by Nucleophilic Reaction of Imidazole Groups with the Electron-Deficient Iodoacetamido Group of the TEMPO Derivative

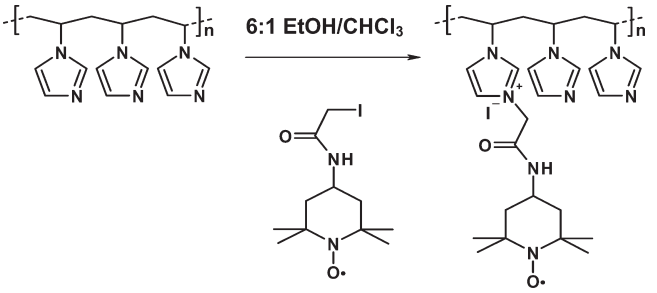

2.2. Experimental Techniques. The electron spin resonance spectra were acquired on a Bruker EMX X-band spectrometer equipped with a rectangular TE102 cavity. The center field was fixed at 0.35 T and the microwave frequency at 9.8 GHz, and the experiments were carried out at 295 K. A modulation frequency of 100 kHz and a field sweep range of 150 G were used. Once the ESR spectra were recorded, the field was fixed at the value of the center peak frequency and the dynamic nuclear polarization (DNP)-enhanced NMR experiments were carried out in the same instrument setup. This was done using a home-built U-shape NMR coil made of 0.010 in. diameter Teflon-coated silver wire tuned to 14.8 MHz and connected to the broadband channel of a Bruker Avance NMR spectrometer. The unpaired electrons are irradiated with a power output between 0.1 mW and 1.5 W continuously using a custom home-built X-band microwave amplifier while the NMR signal was recorded. Dry nitrogen gas was passed over the sample at 9 L/m for cooling the sample. Typical sample volumes used were about 4 μL, and heating effects due to the microwave irradiation even at maximum power were checked to be negligible.[36] The turbidity measurements were carried out using UV−vis spectroscopy at 600 nm using a UV-1800 Shimadzu spectrophotometer with a phosphate buffer as reference. The optical images were taken using differential interference contrast optical microscopy on an Olympus BX60 microscope using a 100× oil immersion lens. Polyaspartate concentrations were determined by amino acid analysis (Beckman 6300 Autoanalyzer) after 24 h hydrolysis in vacuum with 6 M HCl at 110 °C.

3. Theory

3.1. Overhauser Dynamic Nuclear Polarization. The Overhauser-enhanced DNP resulting in the NMR signal enhancement upon irradiation of the electron spin resonance transition is given by[28,37]

$$E = 1 - \rho f s \frac{|\gamma_S|}{\gamma_I} \quad (1)$$

where E is the enhancement of the signal in the presence of microwaves relative to the NMR signal, ρ is the coupling factor reflecting the coupling between the electron and proton, f is the leakage factor describing the influence of

Scheme 2. Synthesis of Sodium Polyaspartate and TEMPO-Labeled Sodium Polyaspartate[a]

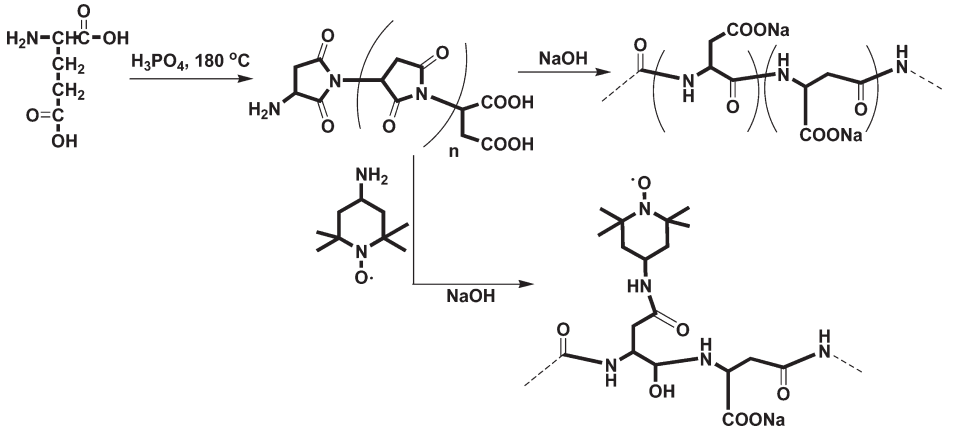

[a] Thermal polymerization of aspartic acid in presence of orthophosphoric acid results in formation of polysuccinimide that undergo nucleophilic reaction with either hydroxyl groups or the amino groups.[35]

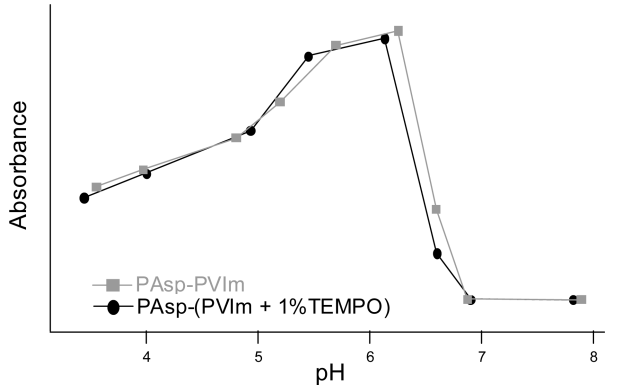

Figure 1. Turbidity (absorbance at 600 nm) as a function of pH during complex coacervation of PAsp with PVIm and PVIm−TEMPO show that functionalization does not affect the complex coacervation phenomena.

electron−proton interaction upon the proton relaxation mechanisms, s is the saturation factor describing the saturation of the electron spin Zeeman transition, and γ_S and γ_I are the magnetogyric ratio of the electron and the proton ($|\gamma_S|/\gamma_I = 658$).

The leakage factor, f, is given by

$$f = 1 - \frac{T_1}{T_{10}} = \frac{kCT_{10}}{1 + kCT_{10}} \tag{2}$$

where T_1 is the longitudinal relaxation of the nucleus in the presence of the electron spins, T_{10} is the longitudinal relaxation of the ^{1}H spins in the absence of the electron spins, C is the concentration of radical, and k is the relaxivity constant. The value of the leakage factor can be accurately determined by measuring the spin−lattice relaxation time of the complex coacervates in both the presence and absence of the spin-labels. Calculating this also takes care of the effects of variable spin-label concentrations in different samples. The saturation factor, s, depends on the B_1 amplitude of ESR irradiation. To eliminate the B_1 strength variations at the sample as a variable, we measured DNP enhancement at a series of B_1 amplitudes and extrapolated it to infinite B_1 strength. The nitroxide radicals possess three hyperfine states due to the ^{14}N having a nuclear spin $I = 1$ interacting with the unpaired electron and the efficiency with which the hyperfine states mix, will affect the saturation factor.[38,39] The efficiency of mixing depends on the amplitude of intermolecular Heisenberg electron spin exchange and the nitroxide's nitrogen nuclear spin relaxation rate. The spin exchange effects can be neglected if intermolecular collision between the spin-labels is hindered, e.g., due to low spin-label concentration or if there is little chance for mutual interaction between the spin-labels. However, it has also been shown that the nitroxide's nitrogen nuclear spin T_1 relaxation times become very low (on the order of a 300−900 ns) if the spin-label's rotational motion is restricted,[40] e.g., when tethered to a macromolecule, and thus can lead to efficient mixing of the hyperfine states. Therefore, even in the absence of Heisenberg spin exchange effects due to low spin-label concentration as is the case in this study, the saturation factor at infinite microwave power, s_{max}, is expected to approach 1 if the spin-labels experience rotational dynamics with correlation times (τ_{rot}) between 7×10^{-10} and 5×10^{-7} s.[39] These correlation times cover the range of the relevant rotational diffusion rates that the spin-labels incorporated on coacervate polyelectrolyte chains have, as can be shown by the fit values of the ESR spectra and discussed in the Results and Discussion section.

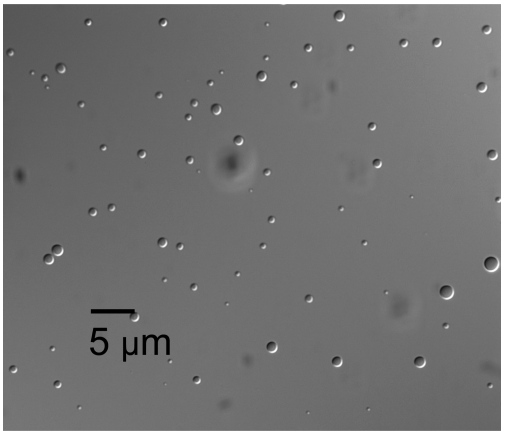

Figure 2. Differential interference contrast optical micrograph (100× magnification) of the coacervate showing the formation of micrometer size complex coacervate droplets at a pH of 5.8.

In order to determine the coupling factor, the DNP enhancements were measured as a function of increasing power and extrapolated to infinite power to obtain maximum enhancement. The relation for maximum enhancement at infinite power is given by

$$E_{max} = E(P \rightarrow \infty) = 1 - \frac{|\gamma_S|}{\gamma_I}\rho f s_{max} \tag{3}$$

Thus, as the maximum enhancement value (E_{max}), the leakage factor (f), and the maximum saturation factor (s_{max}) and the ratio of the magnetogyric ratios are now known, the value of the coupling factor ρ can be determined. Interactions between nitroxide spin-labels and proton water molecules are purely dipolar and have been shown to be dominantly modulated by the translational correlations with negligible rotational contribution due to the absence of a long-lived free electron−proton species, with the help of field cycling relaxometry.[29] For the analysis of the coupling factor we use the spectral density function developed by Hwang and Freed[41] which assumes a hard-sphere, force-free model which is the best approximation for the system of tethered nitroxide spin-labels and the interacting water molecules. This spectral density function relates the coupling factor and the translational correlation time by modeling for the cross-relaxation between the electron and proton spins. It is given by

$$J(\omega,\tau) = \frac{1 + \frac{5\sqrt{2}}{8}(\omega\tau)^{1/2} + \frac{\omega\tau}{4}}{1 + (\omega\tau)^{1/2} + (2\omega\tau) + \frac{\sqrt{2}}{3}(\omega\tau)^{3/2} + \frac{16}{81}(\omega\tau)^2 + \frac{4\sqrt{2}}{81}(\omega\tau)^{5/2} + \frac{(\omega\tau)^3}{81}} \tag{4}$$

In the case of isotropic motion with one translational correlation time τ, which is very much shorter than the electron relaxation times (T_{1e}, T_{2e}), as in the case of tethered nitroxide molecules on macromolecules, the coupling factor is given by[28]

$$\rho = \frac{6J(\omega_S + \omega_I, \tau) - J(\omega_S - \omega_I, \tau)}{6J(\omega_I + \omega_S, \tau) + 3J(\omega_I, \tau) + J(\omega_S - \omega_I, \tau)} \tag{5}$$

Thus, the value of this translational correlation time (τ) can be determined. This correlation time fulfills the relation[28]

$$\tau = \frac{d^2}{D_I + D_S} \tag{6}$$

where d is the distance of closest approach of the two spins, D_I is the diffusion coefficient of the solvent molecules, and D_S is the diffusion coefficient of the electron spin bearing molecules. In our earlier work we have shown that the distance of closest approach, which depends on the van der Waals attraction between the electron and proton, is found to be 4.5 Å at 0.35 T.[32] This was done by calculating the translational correlation time for 4-amino-TEMPO free in solution through DNP and by determining the value of D ($D = D_I + D_S$) from DOSY NMR experiments.[31] As the closest distance to which the ^{1}H of water approach the spin-labels is only limited by the van der Waals forces between them, this distance is not expected to change even if the number of water molecules and collisions were to be sparse. In an independent study using field cycling relaxometry on lipid vesicles systems with spin-labels tethered at various exterior and interior positions of the lipid bilayer, the van der Waals distance of closest approach has been shown to remain around 4.5 Å,[42] although also shorter values of around 2.6 Å have been found for free spin-labels interacting with water.[43,32] It is important to appreciate that errors in the estimation of this distance would only scale the absolute value of the diffusion coefficients. However, the relative changes in the diffusion coefficients that we use to probe the process of complex coacervation as a function of pH would still be accurate. In this paper, we report on the translational correlation time between tethered spin-labels and hydration water determined from the DNP analysis that quantifies solvent diffusion coefficients in the local (4.5 Å) vicinity of the polyelectrolyte tethered spin-labels.

3.2. Electron Spin Resonance. Electron spin resonance is an established technique for the determination of the rotational dynamics of spin-labeled molecular chain segments and local polarity parameters. The basis of this analysis is that the ^{14}N hyperfine splitting constants, a_N, and the g value of nitroxide spin-labels are anisotropic depending on the spatial orientation of the N−O bond with respect to the static magnetic field, B_0. Thus, the ESR line width and line shape are sensitive to the rotational diffusion rate of the spin-labeled segment on the order of 10^6−10^{10} s^{-1} as well as to the anisotropy of the rotational freedom. The hyperfine splitting constant, a_N, is sensitive to polarity profiles and can indirectly reflect water content. This is because the unpaired electron resides closer to the nitrogen or oxygen of the nitroxide depending on the polarity of the environment that stabilizes one of the two configurations ($\rangle^+N^\bullet-O^- \leftrightarrow \rangle N-O^\bullet$). Utilizing these characteristics, literature studies model the a_N parameter to determine hydrogen-bonding contribution in terms of fractional increments relative to pure water.[44,45] However, the interpretation of a_N often does not sufficiently discriminate between the extent of hydrogen bonding due to changing water content and the local solvent polarities or the motional anisotropy. Modeling programs based on the stochastic Liouville equation like nonlinear least-squares (NLSL)[46] and the simulation and fitting program package EasySpin[47] can be used to determine the axial rotational rates of the spin-labels that are covalently attached and thus coupled to the motions of the molecular segments in the coiled polyelectrolyte chains and complex coacervate structures. In our analysis of the ESR spectra with the NLSL program we use g and A tensor elements of $g_{xx} = 2.0089$, $g_{yy} = 2.0062$, $g_{zz} = 2.0032$, $A_{xx} = 6.1$ G, $A_{yy} = 5.9$ G, and $A_{zz} = 33.5$ G and a basis set of truncation with $L^e_{max} = 24$, $L^o_{max} = 14$, $K_{max} = 6$, $K_{min} = 6$.

4. Results and Discussion

Complex coacervation was achieved by mixing 100 mM PVIm ($pK_a = 7.2$) and PAsp ($pK_a = 4.9$) solutions at a pH of about 9 and then slowly reducing the pH by the dropwise addition of 2% HCl. These are the first reports of complex coacervation in this system and result in the appearance of a strong turbidity uniformly across the sample, in the pH range of 6.5−4.8 (Figure 1). The increase in the turbidity only at pH values < 6.5 indicates the requirement of protonated imidazoles to undergo electrostatic interaction with the anionic carboxylate groups on polyaspartate. As shown in Figure 1, the turbidity (measured as an absorbance increase at 600 nm) reaches a maximum around pH 6 and then slowly decreases at lower pH. At a pH below or above this, decreased interaction between the polymers due to the protonation of carboxylates or deprotonation of imidazoles, respectively, results in lower turbidity. The turbidity curves for PVIm−PAsp and for TEMPO-functionalized PVIm−PAsp were found to be similar (Figure 1), which indicates that TEMPO spin-labels do not interfere with the coacervation process.

The existence of fluidic coacervate droplets was confirmed through differential interference contrast optical microscopy of the complex coacervate phase, showing perfectly spherical, submicrometer size droplets dispersed in solution at a pH of 5.8 (Figure 2). This direct visual evidence of the formation of well-defined and perfectly spherically shaped complex coacervates proves their liquid character. These droplets show a size distribution with diameters varying from about 0.2 to 1 μm. No aggregates were observed below pH 4.0 or above pH 6.5 by optical microscopy.

To study the solvent microviscosity upon complex coacervation, the local water diffusion coefficients were quantified via DNP experiments with either of the polyelectrolytes functionalized. The measured DNP enhancements have an opposite sign in comparison to the NMR signal intensity because of the dipolar nature of the electron−proton interaction. The maximum (negative) enhancements as a function of the pH have been plotted on the top panel of Figure 3. Interestingly, at high pH the enhancements are close to −10-fold in the case of TEMPO-labeled PVIm, while they have a much lower enhancement value of about −6-fold for TEMPO-labeled PAsp. The differences in the enhancements for PVIm and PAsp are due to the differences in the water mobility at the different polyelectrolyte surfaces, which can arise due to different charge density, hydrophobicity, or structure of the individual polymers. For both polyelectrolytes, the high values of the enhancement reflect fast water dynamics on the surface of these polyelectrolytes which mainly exist in a relatively extended configuration under these conditions. As the pH is reduced, the polymer chains interact, leading to the formation of the complex coacervate microspheres at a pH of ~5.8. This leads to a gradual decrease in the maximum enhancement values and finally a very low-amplitude negatively amplified NMR signal under fully coacervating conditions. As the pH is further reduced, the enhancements start to increase again as the polyelectrolytes now separate out from the complex coacervate phase into a more stretched configuration. This happens because at low pH, PVIm becomes completely protonated and hence prefers an extended conformation, whereas PAsp would separate out and undergo hydrogen-bonding between the carboxylates through inter- or intra-PAsp interactions. Significantly, the trend of maximum DNP enhancements reproduces the behavior of the turbidity curve. It is important to appreciate that while turbidity is a measure of the formation of macroscopic molecules of the order of the incident wavelength (600 nm) used, the DNP technique probes the local water mobility and its interaction with the spin-labels within 5−10 Å distances and thus changes at a much smaller length scales or much smaller complexes.

From these maximum enhancement values, the coupling factors were determined after measuring the leakage factors and inserting $s_{max} = 1$ into eq 3 and plotted as a function of

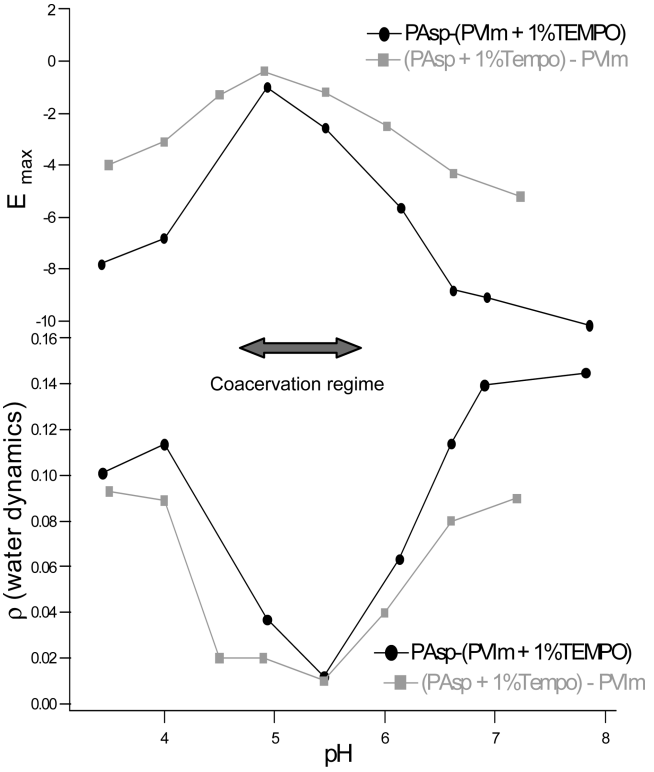

Figure 3. Upper panel: the value of maximum enhancement obtained as a function of pH for functionalized PVIm and PAsp. Lower panel: the corresponding values of ρ (coupling factor) determined using eq 33, plotted for different pH.

pH on the lower panel of Figure 3. The coupling factors enable the estimation of the translational correlation time between the locally interacting protons of water and electron spins through the spectral density function, as discussed in the Theory section. As shown in eq 6, from the value of the translational correlation times and the distance of closest approach (4.5 Å), the sum of the diffusion coefficients of the spin-labels and the local water molecules can be determined. As the water diffusion coefficients are more than 1 order of magnitude larger than the diffusion coefficients of tethered spin-labels, the total diffusion coefficient is attributed to the hydration water alone.

The calculated values for the diffusion coefficients of this hydration water are plotted in Figure 4. At low and high pH where no complex coacervation occurs, the values on the surface of uncomplexed polyelectrolytes are $(1.2-1.6) \times 10^{-9}$ m^2/s, showing differences between PVIm and PAsp. To our knowledge, these are the first quantitative measurements of diffusion constants of the local water interacting with extended chain polyelectrolyte surfaces under ambient solution state conditions. (The bulk water self-diffusion coefficient of 2.3×10^{-9} m^2/s has been drawn as a reference in Figure 4). The hydration water diffusion coefficient gradually reduces as complex coacervation occurs and merges into a single value of 0.25×10^{-9} m^2/s in the coacervation regime. One question that remains to be answered is whether this value is reporting on the internal and local polyelectrolyte surface water dynamics inside complex coacervates, as opposed to effects of bulk water-exposed or residual uncomplexed polyelectrolytes. The micrometer-sized complex coacervate droplets result in a large internal surface area that the spin-labels are probing in comparison to their external surface area, which addresses one issue, namely that effects of spin-labels probing the bulk water-exposed polyelectrolytes on the surface of complex coacervate droplets can be neglected. Another issue is whether the DNP enhancements originate from a small fraction of uncomplexed

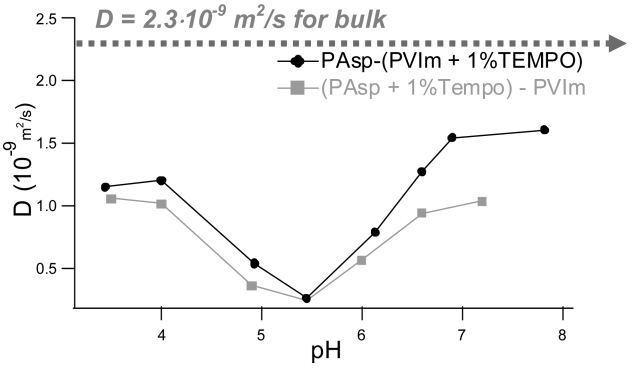

Figure 4. Diffusion coefficients of the water close to the coacervated spin-labeled polyelectrolytes as a function of pH, determined from the DNP analysis. The dotted line represents bulk water self-diffusion coefficient. The errors in the calculated values of the diffusion coefficients are less than 15%.

polyelectrolytes? As will be discussed further below, the ESR analysis of the dilute equilibrium phase, physically separated from the coacervate phase, concluded that there remains a residual fraction of small polyelectrolyte species but that even these small polyelectrolyte species exist as coacervated complexes at this pH of ~5.5. We also measured local water dynamics of this physically separated dilute phase and found that the local water dynamics was significantly reduced compared to that in complex coacervate solution. This is in agreement with the idea that the measured dynamics (0.25×10^{-9} m^2/s) does not arise from and is not affected by uncomplexed polyelectrolytes (that would be entirely contained in the dilute phase) and that the dilute phase contains residual complexed polyelectrolytes. We can thus safely assume that the polyelectrolyte-tethered spin-labels are reporting on the characteristics of water in the interior of complex coacervates. This also shows that the complete physical separation of the dilute phase with no residual coacervated complexes is difficult or perhaps impossible.

The calculated diffusion coefficient of 0.25×10^{-9} m^2/s is an order of magnitude smaller than that of bulk water, suggesting restricted diffusion of the water in the pore spaces in the interior of complex coacervates. This value however also indicates that this is not structurally bound water moving with the diffusion coefficient of the polyelectrolytes but is water confined in nanoscale pore spaces within the coacervate (e.g., self-diffusion of poly(diallyldimethylammonium chloride and protein bovine serum albumin coacervates has been reported to be of the order of $10^{-12}-10^{-14}$ m^2/s[17]). Previous fluorescence anisotropy studies on a very comparable coacervating system of PVIm−ALG (sodium alginate) using pyrene-labeled PVIm showed that polarity reduced during coacervation due to desolvation. However, the polarity value in the fully coacervated phase shows that there is still substantial water in the coacervates, an observation that is in agreement with our analysis. The same study also showed PVIm and ALG to be homogenously distributed in the coacervates at 100 nm resolution, implying water to be confined at length scales smaller than this 100 nm length scale.[34]

Our observation is that when PVIm or PAsp is uncoacervated, the surface diffusion coefficients measured using spin-labels are different. These coefficients merge into one single value upon coacervation, indicating that PVIm and PAsp assume homogeneous structures and that the different labels are exposed to similar environments inside the coacervate microspheres. As explained above, in the case of PVIm−ALG, with each polymer labeled with a different color dye, it was shown using confocal microscopy that the oppositely charged polymers come together and are highly condensed throughout the microspheres, forming what appears to be a homogeneous phase on a 100 nm grid.[34]

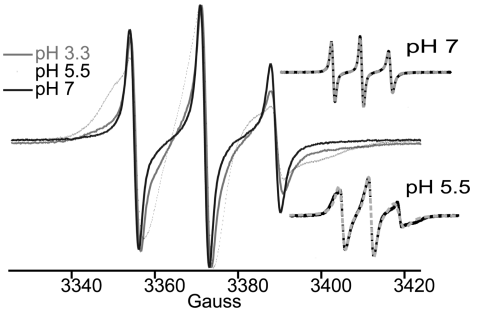

Figure 5. ESR curves obtained for TEMPO-labeled PAsp, plotted at three different pH, showing the line broadening features at coacervation and less broad, isotropic spectra at higher and lower pH. Top inset shows the ESR curve (black line) at pH 7 fit using the NLSL program (gray dashes) while the bottom inset shows the ESR curve (black dots) with the faster components spectrally subtracted, at pH 5.5, fit using the NLSL program (gray dashes).

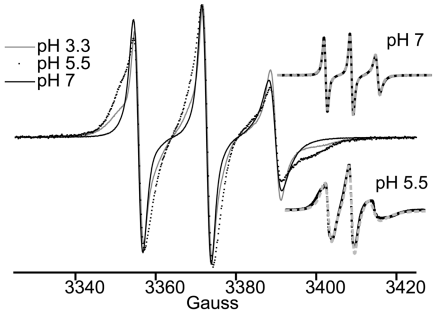

Figure 6. ESR curves for PVIm−TEMPO plotted as a function of pH showing the line broadening features at coacervation and less broad, isotropic spectra at higher and lower pH for the case of PVIm. Top inset shows the ESR curve (black line) at pH 7 fit using the NLSL program (gray dashes) while the bottom inset shows the ESR curve (black dots) with the faster components spectrally subtracted, at pH 5.5, fit using the NLSL program (gray dashes).

However, only the molecular-level analysis presented here of polymer surface water dynamics on the sub-nanometer length scale can confirm that indeed the individual polycation and polyanion monomers assume similar configurations when they are complexed and coalesce into coacervates.

One of the key assumptions in our DNP evaluation of the diffusion coefficients is that there exists fast exchange of the water molecules between the hydrated coacervate interior and bulk water. The spin−lattice relaxation time of the water molecules being on the order of 2 s warrants the polarization build-up time for DNP to be about 10 s. Thus, these long build-up times together with the measurement of fast moving water molecules ($\sim 0.25 \times 10^{-9}$ m^2/s) ensure that the water has fully exchanged between the coacervate and equilibrium phase. Even in the unlikely event that the water diffusion constant is on the order of 10^{-12} m^2/s (e.g., for structurally bound water), the root-mean-square displacements in one second would be $\sim 2.5\ \mu$m, i.e., larger than the complex coacervate droplets. So, the water would have exchanged in and out of the coacervate droplets even in this scenario. In addition, the distribution of bulk self-diffusion coefficients of water were measured using pulsed-field-gradient NMR experiments with 300 ms observation durations, and only a single population for the self-diffusion coefficient of water was observed. Also, careful measurements of T_1 NMR relaxation times present a purely monoexponential decay for ^{1}H signal of water. Because both relaxation and diffusion coefficients of water inside the coacervate droplets and dilute solution are measurably different, only full exchange of water in and out of coacervates within the observation times (a few hundred milliseconds to seconds) can support these observations.

The ESR spectra for spin-labeled PVIm and PAsp are plotted in Figures 5 and 6. Spectra of both polyelectrolytes highlight the fact that the ESR lines significantly broaden at the maximum coacervation pH of ~5.5, over a narrow pH range, due to restriction in the motional freedom of the complexed polyelectrolytes within the coacervates (Figures 5 and 6). The ESR line width above and below this narrow coacervation regime is significantly narrower and displays isotropic, motionally narrowed features that are distinctly different from the ESR spectra of the complexed polyelectrolytes. The ESR spectra at pH 5.5 of the coacervated phase are dominated by a slower rotational component, while there exists a small fraction of faster components. The latter could be from either a small fraction of uncomplexed polyelectrolytes or significantlyer smaller sized coacervate complexes . To better understand the nature of this faster rotational components, we carried out the physical separation of the dilute equilibrium phase from the complex coacervates by centrifugation of the turbid coacervate solution at 5000 rpm for 60 min. As expected, the supernatant was entirely transparent, and no coacervate droplets (such as those in Figure 2) were visible under the microscope. However, amino acid analysis of the aspartic acid content in the supernatant showed that about 9% of the total polyelectrolytes remained in the supernatant. To verify the nature of this supernatant, ESR analysis was carried out on this phase. The analysis revealed the characteristic broadened spectrum with features indistinguishable from that of the coacervate phase, except that the signal amplitude was much lower. This provides evidence that all polyelectrolytes detected in the supernatant at pH 5.5 still exist as polyelectrolyte complexes, as further supported by DNP analysis discussed above. If there was a measurable contribution from uncomplexed polyelectrolytes, the supernatant should hold a higher fraction of these free polyelectrolytes and thus present different ESR spectra with more pronounced narrow features and display higher DNP enhancements. This study also confirms that the complete physical separation of this delicate liquid−liquid colloid solution is difficult if not impossible.

Careful ESR analysis of the spin-label dynamics has been carried out to characterize the changes in side-chain packing and the local polymer segmental motion during the process of complex coacervation. As the spin-labels are covalently attached three bond lengths away to the polymer segments, it is not possible to attribute all the motion of the spin-label to the polymer segment alone because the spin-label motion is not perfectly coupled to the local polymer segment motion. Therefore, the ESR features represent the dynamics of the spin-label itself that corresponds to side-chain packing, mixed with influences of the local segmental mobilities. The spin-label dynamics will still be influenced by the local segmental mobilities, which is evident from the fact that even within the noncoacervation regime at high and low pH, there are gradual changes in the rotational dynamics as a function of pH that is expected to change the polymer dynamics/compactness by changes of the charge density (Figures 7 and 8). In this regime, although interpolymer interactions are present, the fraction of uncomplexed polyelectrolytes is too large that the EPR line broadening cannot be merely attributed to spin-label interactions. However, because we are reporting on the process of complexation and not on the absolute dynamics of our polyelectrolyte system by itself, even the side-chain mobility alone sensitively and directly report on polyelectrolyte packing. Using the NLSL analysis as described in the Experimental Methods section to fit the ESR spectra, the perpendicular ($R_\perp$) and parallel ($R_\parallel$) rotational diffusion rates of the spin-labels relative to their long axis are obtained and plotted in Figures 7 and 8. We observe that the rotational diffusion of the spin-labels as part of the uncoacervated polyelectrolyte is high, on

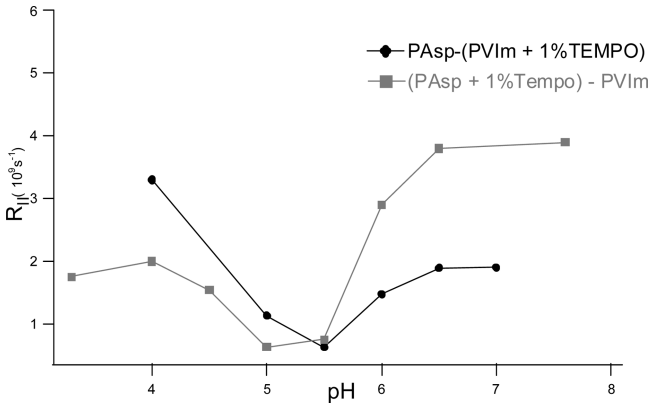

Figure 7. Rotational correlation time parallel to the axis for functionalized PVIm and PAsp as a function of pH, obtained by fitting the ESR spectra with the help of the NLSL program.

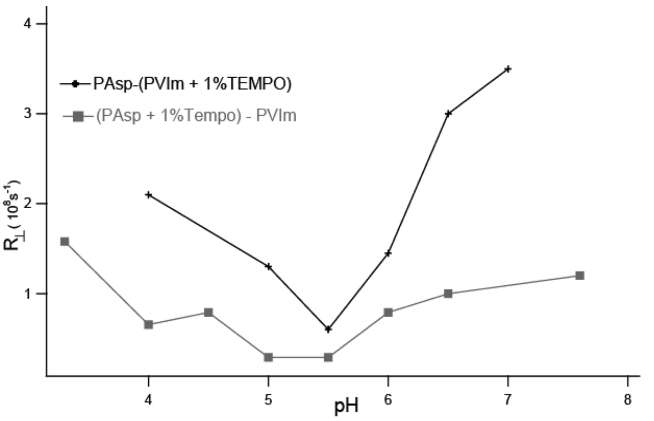

Figure 8. Rotational correlation time perpendicular to the probe axis for functionalized PVIm and PAsp as a function of pH, obtained by fitting the ESR spectra with the help of the NLSL program.

the order of $1-5 \times 10^8\ s^{-1}$, and differs between PVIm and PAsp. When complex coacervation occurs, the rotational diffusion coefficients of the spin-labels attached to both polymers consistently decrease by a factor of 5 (Figures 7 and 8). Analogous to the observation on the surface hydration dynamics, the spin-label dynamics and thus the side chain and polymer segment mobility of both polycations and polyanions show dissimilar characteristics when uncoacervated and comparable characteristics when coacervated. This further supports the picture that spin-labels on PVIm and PAsp experience largely similar environments within the complex coacervate microdroplets. Furthermore, one can obtain the dynamic anisotropy parameter, which is the ratio of the parallel and perpendicular rotational rates ($N = R_{||}/R_{\perp}$), which again shows the 5-fold change from the uncoacervated to coacervated phase. Again, the discussed values represent a combined effect of mobility changes in side chain and polymer segment anisotropy.

Finally, we would like to discuss the highly fluidic nature of the extremely condensed complex coacervate phase. The high polymer concentration of the equilibrium solution of 50 mM further greatly increases in the complex coacervate phase due to significant condensation occurring during the polyelectrolyte phase separation. Assuming the coacervates to have a uniform concentration throughout the solution and using the differential interference optical microscopy images, we approximated the upper ceiling for the polymer density in the coacervate molecules. Assigning 90% of the entire polyelectrolyte concentration of the image to be distributed in the coacervate spheres, a density of 1.7 g/mL for the complex coacervates was estimated. This was done by calculating a volume of 1554 μm^3 for the field of view of the optical image assuming a thickness of 1 μM, as this thickness is estimated to be similar to that of the largest microspheres formed. The total volume in the coacervates was calculated by adding up the volume of each of the coacervate spheres in the field of view and it is found to be around 19.5 μm^3. Given this high density, it is peculiar that the complex coacervates not only are fluidic but also display high side-chain mobility and polymer segment rotational diffusion whose dynamics are comparable to that found in liquid crystals and only changes ~5-fold compared to the equilibrium solution. Interestingly, in a previous study, fluorescence anisotropy of pyrene-labeled PVIm−ALG coacervates also showed that the microviscosity of fluorescence probe dynamics changed by ~5-fold from equilibrium solution to the complex coacervated phase.[34] The experimental confirmation of the same characteristic changes in comparable polyelectrolyte systems using two completely different spectroscopic probes provides strong support for the validity of our observation.

5. Conclusions

The homopolycation PVIm (74 kDa) and polyanion PAsp (60 kDa) undergo complex coacervation in the pH range 6.5−4.5, where the polycation and polyanion are largely charge-matched. We applied a novel DNP-amplified ^{1}H NMR method for the first time and quantified the surface hydration dynamics within 5−10 Å of spin-labels covalently bound to polyelectrolytes, in equilibrium solution as well as in the complex coacervates. The finding was that both polyelectrolytes are significantly hydrated and exhibit high water mobility on their surfaces when uncomplexed and freely dissolved ($D \sim (1.2-1.6) \times 10^{-9}$ m^2/s), although to a slightly different extent, and that the hydration water gets confined in nanometer-scale pores when they form the coacervates, displaying a 5−6-fold decrease in the local solvent diffusion coefficients, to a value of $D \sim 0.25 \times 10^{-9}$ m^2/s. Consequently, there exists a measurable fraction of dynamic, freely exchanging, water inside the coacervate microdroplets. One implication of this finding is that PVIm−PAsp coacervate systems would be responsive to solvent-mediated stimuli, such as pH or salt. Using the same spin-labeled polyelectrolyte samples, the coupled spin-label and polymer segmental rotational diffusion coefficients were determined utilizing CW ESR spectral analysis, and they were shown to have a ~5-fold decrease in mobility in the complex coacervate phase compared to equilibrium solution. Both the solvent and polymer dynamics measurements show similar characteristics for either polyelectrolyte when coacervated, although their characteristics as uncoacervated and thus separate polyelectrolytes differ measurably. CW ESR analysis also showed that almost all polyelectrolytes concentrate into the coacervate droplets, depleting the equilibrium solution phase of free polyelectrolytes. Analysis of the supernatant after separating out the complex coacervate phase indicated that there still existed residual polyelectrolytes, however not as hydrated and/or monomeric species but as smaller complexed coacervates. This shows the limitation of the physical analysis of coacervate characteristics upon physical phase separation and highlights the importance of novel noninvasive techniques like DNP and ESR analysis. On the basis of this finding and using differential interference optical microscopy images with sharp contrast, an upper ceiling for the polyelectrolyte density in coacervates was estimated to be 1.7 g/mL. We conclude that PVIm and PAsp form a condensed and homogeneous coacervate phase, and furthermore, pairwise complexation of PVIm and PAsp is likely to occur. Only roughly pairwise combined, thus largely charge compensated, species can further assemble to such dense complexes that display high solvent and polymer dynamics, although they are composed of highly charged components. Also, pairwise,

local-level complexation can explain the similar spin-label mobilities and water diffusion coefficients in the local vicinity of either polyelectrolytes when complex coacervated, although they display measurably different local solvent and spin-label mobilities when uncomplexed. Characteristics reported for a comparable system of PVIm−ALG complex coacervates show similar trends and support our finding.[34] This is in sharp contrast to the coacervation between globular proteins and extended polyanion systems, such as whey protein and gum arabic,[16,48] wherein the polymer segment viscosity within coacervates increases by ca. 45-fold from equilibrium solution. A plausible explanation is that such differing structures cannot display effective charge neutralization even with pairwise complexation, so that the presence of stronger electrostatic interaction makes the complexes act as polar species at high concentration and not as quasi-hydrocarbons. Thus, we present the first study on the locally interacting solvent on the polyelectrolyte surface and the spin-labels covalently bound to polyelectrolyte segments themselves and further show the relevance of such dynamic parameters not only to applications but also for gaining insight into the structure or mechanisms of complex coacervation.

Acknowledgment. This work was supported by the MRL program of the National Science Foundation (NSF) under Grant DMR05-20415 and partially by the NSF Faculty Early CAREER Award (CHE-0645536) of Han and the Packard Fellowship for Science and Engineering awarded to Han. Waite was supported by an NIH grant (R01DE 018468). Korevaar was supported by the NSF Division of Materials Research through the CISEI program and IMI programs and Eindhoven University of Technology. Brian Matsumoto (UCSB) is thanked for the optical microscopy. The authors also thank Peter Allen for the TOC graphic, Brandon Armstrong for helpful discussions, and April Sawvel for helping us initiate this collaboration.

References and Notes

(1) Bungenberg de Jong, H. G. In *Colloid Science*; Kruyt, H. R., Ed.; Elsevier: Amsterdam, 1949; Vol. *II*, Chapters VIII and X.
(2) Turgeon, S. L.; Beaulieu, M.; Schmitt, C.; Sanchez, C. *Curr. Opin. Colloid Interface Sci.* **2003**, *8* (4−5), 401–414.
(3) Tiebackx, F. W. Z. *Chem. Ind. Kolloide* **1911**, *8*, 198–201.
(4) Bungenberg de Jong, H. G.; Kruyt, H. R. *Proc. K. Ned. Akad. Wet.* **1929**, *32*, 849–856.
(5) Oparin, A. I. *The Origin of Life*; Dover Publications: New York, 1953.
(6) Bakker, M. A. E.; Konig, M. M. G.; Visser, J. Fatty Ingredient, World Patent Application WO94/14334, **1994**.
(7) Kester, J. J.; Fennema, O. R. *Food Technol.* **1986**, *40* (12), 47–59.
(8) Schmitt, C.; Sanchez, C.; Desobry-Banon, S.; Hardy, J. *Crit. Rev. Food Sci. Nutr.* **1998**, *38* (8), 689–753.
(9) Burgess, D. J. Complex Coacervation: Microcapsule Formation. In Dubin, P. L., et al., Eds.; *Macromolecular Complexes in Chemistry and Biology*; Springer-Verlag: Berlin, 1994; Chapter 17, pp 285−300.
(10) Chilvers, G. R.; Morris, V. J. *Carbohydr. Polym.* **1987**, *7* (2), 111–120.
(11) Daniels, R.; Mitermaier, E. M. *J. Microencapsulation* **1995**, *12* (6), 591–599.
(12) Ijichi, K.; Yoshizawa, H.; Uemura, Y.; Hatate, Y. *J. Chem. Eng. Jpn.* **1997**, *30* (5), 793–798.
(13) Luzzi, L. A. *J. Pharm. Sci.* **1970**, *59* (10), 1367–1376.
(14) Zhao, H.; Sun, C. J.; Stewart, R. J.; Waite, J. H. *J. Biol. Chem.* **2005**, *280*, 42938–42944.
(15) Waite, J. H.; Andersen, N. H.; Jewhurst, S.; Sun, C. J. *J. Adhes.* **2005**, *81*, 297–317.
(16) Weinbreck, F.; Rollema, H. S.; Tromp, R. H.; de Kruif, C. G. *Langmuir* **2004**, *20*, 6389–6395.
(17) Menjoge, A. R.; Kayitmazer, A. B.; Dubin, P. L.; Jaeger, W.; Vasenkov, S. *J. Phys. Chem. B* **2008**, *112*, 4961.
(18) Kramer, G.; Somasundaran, P. *J. Colloid Interface Sci.* **2004**, *273*, 115–120.
(19) Liz, C. C. C.; Petkova, V.; Benattar, J. J.; Michel, M.; Leser, M. E.; Miller, R. *Colloids Surf., A* **2006**, *282*, 109–117.
(20) Schmitt, C.; Sanchez, C.; Lamprecht, A.; Renard, D.; Lehr, C. M.; de Kruif, C. G.; Hardy, J. *Colloids Surf., B* **2001**, *20*, 267–280.
(21) Leisner, D.; Imae, T. *J. Phys. Chem. B* **2003**, *107*, 8078–8087.
(22) Menger, F. M.; Peresypkin, A. V.; Caran, K. L.; Apkarian, R. P. *Langmuir* **2000**, *16*, 9113–9116.
(23) Menger, F. M. *Proc. Natl. Acad. Sci. U.S.A* **2002**, *99*, 4818–4822.
(24) Khoshtariya, D. E.; Hansen, E.; Leecharoen, R.; Walker, G. C. *J. Mol. Liq.* **2003**, *105*, 13–36.
(25) Gawrisch, K.; Gaede, H. C.; Mihailescu, M.; White, S. H. *Eur. Biophys. J.* **2007**, *36*, 281–291.
(26) Ge, M. T.; Freed, J. H. *Biophys. J.* **2003**, *85*, 4023–4040.
(27) Finer, E. G.; Darke, A. *Chem. Phys. Lipids* **1974**, *12*, 1–16.
(28) Hausser, K. H.; Stehlik, D. *Adv. Magn. Reson.* **1968**, *3*, 79–139.
(29) Borah, B.; Bryant, R. G. *J. Chem. Phys.* **1981**, *75* (7), 3297–3300.
(30) Halle, B. *J. Chem. Phys.* **2003**, *119*, 12372–12385.
(31) McCarney, E. R.; Armstrong, B. D.; Kausik, R.; Han, S. *Langmuir* **2008**, *24*, 10062–10072.
(32) Armstrong, B. D.; Han, S. *J. Am. Chem. Soc.* **2009**, *131*, 4641–4647.
(33) Armstrong, B. D.; Soto, P.; Shea, J. E.; Han, S., submitted to *J. Magn. Reson.*
(34) Srivastava, A.; Waite, J. H.; Stucky, G.; Mikhailovsky, A. *Macromolecules* **2009**, *42*, 2168–2176.
(35) Neri, P.; Antoni, G.; Benvenuti, F.; Cocola, F.; Gazzei, G. *J. Med. Chem.* **1973**, *16*, 893–897.
(36) Armstrong, B. D.; Lingwood, M. D.; McCarney, E. R.; Brown, E. R.; Blümler, P.; Han, S. *J. Magn. Reson.* **2008**, *191* (2), 273–281.
(37) Muller-Warmuth, W.; Meise-Gresch, K. *Adv. Magn. Reson.* **1983**, *11*, 1–45.
(38) Bates, R. D.; Drozdoski, W. S. *J. Chem. Phys.* **1977**, *67*, 4038–4044.
(39) Armstrong, B. D.; Han, S. *J. Chem. Phys.* **2007**, *127*, 104508–10.
(40) Robinson, B. H.; Haas, D. A.; Mailer, C. *Science* **1994**, *263*, 490–493.
(41) Hwang, L.-P.; Freed, J. H. *J. Chem. Phys.* **1975**, *63* (9), 4017–4025.
(42) Hodges, M. W.; Cafiso, D. S.; Polnaszek, C. F.; Lester, C. C.; Bryant, R. G. *Biophys. J.* **1997**, *73*, 2575–2579.
(43) Hofer, P.; Parigi, G.; Luchinat, C.; Carl, P.; Guthausen, G.; Reese, M.; Carlomagno, T.; Griesinger, C.; Bennati, M. *J. Am. Chem. Soc.* **2008**, *130*, 3254–3255.
(44) Marsh, D. *Proc. Natl. Acad. Sci. U.S.A.* **2001**, *98* (14), 7777–7782.
(45) Marsh, D. *Eur. Biophys. J.* **2002**, *31* (7), 559–562.
(46) Budil, D. E.; Lee, S.; Saxena, S.; Freed, J. H. *J. Mag. Reson., Ser. A* **1996**, *120*, 155–189.
(47) Stoll, S.; Schweiger, A. *J. Magn. Reson.* **2006**, *178*, 42–55.
(48) Weinbreck, F.; de Vries, R.; Schrooyen, P.; de Kruif, C. G. *Biomacromolecules* **2003**, *4* (2), 293–303.